Int. J. Electrochem. Sci., 15 **(2020)** 7994 – 8011, doi: 10.20964/2020.08.59

International Journal of
ELECTROCHEMICAL
SCIENCE
www.electrochemsci.org

Anticorrosive Characteristics of Electrodeposited PASP/ Ox-MWNT composite on Carbon Steel in Hydrochloric Acid

A. G. Al-Gamal[1], *M.H. Al-Damasy*[1,2], *K.M. Hashem*[1], *E.G.Zaki*[1], *M. AbdEl-Raouf*[1*].

[1] Egyptian petroleum Research Institute, Nasr City, Cairo (11727), Egypt
[2] Helmholtz-Zentrum Berlin für Materialien und Energie, Kekuléstraße 5, 12489 Berlin, Germany
[*]E-mail: Abdelraouf1979@yahoo.com

Received: 20 July 2019 / *Accepted:* 1 May 2020 / *Published:* 10 July 2020

A composite from poly aspartic acid with oxidized multi-walled nanotubes (PASP/Ox-MWNTs) was electrochemically deposited on carbon steel, and then it was investigated as an anti-corrosion coating. Anti-corrosion action of PASP/Ox-MWNT deposited layers was evaluated using electrochemical methods as electrochemical impedance spectroscopy (EIS) and potentiodynamic polarization in HCl (1M) at different applied voltages. Covering the surface by PASP/Ox-MWNTs resulted in a negative shift in the corrosion potential (E_{corr}) demonstrating that the PASP/Ox-MWNTs can hinder the corrosion reaction. Finally, SEM was used to study the morphology of surfaces covered with and without PASP/Ox-MWNTs after immersion in HCl (1M). Observed results are presented and discussed here.

Keywords: Carbon nanotubes; Composite; Electrodeposition; poly aspartic acid; EIS.

1. INTRODUCTION

Carbon steels are a wide range of metal alloys made from a mixture of carbon and iron. They are one of the most extensively used iron alloys for industrial and engineering purposes. Due to its favorable characteristics like weldability, formability, low cost, and mechanical strength, carbon steels are always the choice in many applications like nuclear power plants, scientific devices, and petroleum production and processing utilities [1]. Although carbon steels have a myriad of advantages, it also has a major drawback, which is its weak resistance to corrosion. Most of the industrial environments in which carbon steel alloys were utilized are harsh and contain aggressive corrosive elements, like offshore petroleum platforms and submerged instruments in petroleum wells [2-4]. Corrosion becomes inevitable for metal surfaces exposed to aggressive species like hydroxide and chloride ions. So, uncovered surfaces in such an environment have to be coated to be maintained and to avoid big economic loses [5].

Since Iijima discovered them in 1991, carbon nanotubes (CNTs) were evolved from intensive laboratory work to potential industrialized uses due to its exceptional electrical, morphological and mechanical properties [6, 7]. Virgin CNTs naturally combine in bundles due to van der Waals attraction between the outer walls of the tubes [8-10]. CNTs ought to be soluble in aqueous solution to be deposited electrochemically as a coat for corrosion protection of carbon steels, so CNTs have to be bundled into single tubes, and this could be done through functionalizing the outer walls of the tube. Two types of functionalization were reported, covalent and non-covalent functionalization. Covalent functionalization contains an electron transferring among CNTs and the organic reactant, and the resulted bond is permanent. Moreover, it harms CNTs and damages its electronic properties [11, 12]. Non-covalent functionalization which is based on weak interactions between functional groups and CNTs particles and it has the advantage of keeping the intrinsic electronic properties of CNTs. Moreover, it is easy, economical and maintains the cylindrical structure of CNTs [13-15]. In this context, researchers have been tested various materials to reduce van der Vaal interactions between CNTs and consequently to achieve a highly dispersed CNTs in different media [16, 17]. Various biomolecules such as proteins [18], peptides [19], polysaccharides [20] and DNA [21], moreover they tested different types of surfactants [22] and polymers [23, 24].

In this study, a composite from poly aspartic acid with Oxidized multi-walled nanotubes (PASP/Ox-MWNTs) was electrochemically deposited on carbon steel, and then it was investigated as an anti-corrosion coating. Moreover, a try to develop the research domain of highly dispersed CNTs by using poly aspartic acid (PASP) as a potential amino acid through covalent functionalization was reported [25]. The interactions of PASP with Ox-MWNTs are studied using FTIR, TGA analysis, and TEM micrographs.

2. EXPERIMENTAL

2.1. Chemicals and Materials

Multi-Walled carbon nanotubes (MWNTs) were synthesized at Nanomaterial research center at Egyptian Petroleum Research Institute (EPRI), > 85% purity, 10-40 nm diameter, length 10-50 μm, and the number of walls about 40-50) and were prepared by chemical vapor deposition then purified according to [26]. HNO_3 (37%), H_2SO_4 (98%), HCl (37%), organic solvent including Dimethylformamide (DMF), toluene and ethanol were brought from Honeywell Co. (USA). L-aspartic acid (molecular formula: $C_4H_7NO_4$ and molar mass: 133.1 g/mol) and $ZrCl_4$ (molecular weight: 233.04 g / mol) were purchased from Merck German company. Poly aspartic acid (PASP) with molecular weight ~ 1000-5000 g/mol was prepared by eco-thermal polymerization of L-aspartic acid according to previous reported works [27 and 28]. All PASP/Ox-MWNTs different suspensions were prepared in distilled water as a medium.

2.2. Functionalization of Ox-MWNTs with PASP

MWNTs first was functionalized with PASP. Accordingly, pristine of MWNTs was mixed with acids mixture H_2SO_4–HNO_3 (3:1 volume ratio) at 60 ^{0}C for 24 h to prepare oxidized MWNTs (Ox-MWNTs). It is famous that acids mixture well serves as strong oxidizing agent for carbon tube surface due to presence nitronium ions NO_2^+ which attack the aromatic ring of outer MWNTs layer leads to oxidation of tubes edges and ends [29 and 30]. Then, the suspension was filtered using a vacuum-sintered glass Buchner funnel and concurrently washed with de-ionized water. Subsequently, 1 g Ox-MWNTs and 1 g PASP acid in 250 ml DMF and 25 ml toluene is exposed to ultrasonic waves for two h and stirred for 12 hrs under atmospheric pressure. For the reaction catalyzation, $ZrCl_4$ (5% mol.) is added to the reaction medium [31]. The obtained suspension is filtered using PTFE membrane and washed with deionized water and THF repeatedly to eliminate any unreacted amino acid molecules. Ultimately, the composite was dried in the oven at 50 ^{0}C for two days.

2.3. Electrode Pretreatment

The carbon steel working electrode with a surface area of 1.0 cm^2 was prepared according to ASTM G31standard method. Briefly, the surface of the samples was excessively refined by iron emery motor followed by emery papers (1200 grit), degreased and cleaned with acetone ultrasonically and stored in a dry atmosphere. Table 1 shows the carbon steel chemical composition that was used in this study.

Table 1. Chemical composition of carbon steel.

Element	**Fe**	**C**	**Si**	**Mn**	**Mo**	**P**	**S**	**Ni**	**Cr**	**Cu**
(W %)	96.12	0.13	0.42	1.58	0.74	0.04	0.03	0.31	0.31	0.33

2.4. Electrochemical Deposition

First, the electrolyte solution was prepared by dissolving the tiny quantity of sodium chloride to make solution conduct the current. Following by adding and 2 g of PASP/Ox-MWNTs composite in 250 ml distilled water by vortexing. Second, the solution was sonicated for 30 minutes in an ultrasonic bath sonicator to disperse the nanocomposite to the maximum limit. Third, the carbon steel set as an anode, a Pt wire as a cathode and a DC power supply model LB 81 was utilized for the electrochemical deposition of PASP/Ox-MWNTs composite, the possible mechanism for the deoxygenation process of terminal carboxylic groups at the anode is well reported by Ruoff et al. [32]. Sodium chloride reactions occurred at both electrodes is ignored because of its negligible portion compared with PASP/Ox-MWNTs composite in the prepared electrolyte solution. The applied voltages were 3, 6, 9 and 12 V to prepare different samples with different electrodeposition conditions Sample-3V, Sample-6V, Sample-9V, and Sample-12V respectively. Eventually, coated prepared samples were taken away from the

deposition medium and placed overnight at 40 °C in a vacuum oven to evade corrosion due to water molecules penetrations through the deposited films.

2.5. Analysis Techniques

Structures of Ox-MWNTs and PASP/Ox-MWNTs were characterized by Fourier transform infrared spectroscopy (FTIR), FTIR samples were analyzed using [Thermo Fisher Scientific; Nicolet iS10 FTIR spectrometer, USA] with measuring range from 400–4000 cm^{-1} and 4 cm^{-1} resolution. The TGA of the prepared PASP/Ox-MWNTs composite was done at a temperature range of 25°C–800°C using SDT Q600 V20.5 Build 15 at a heating rate of 10°C/min under air atmosphere. The surface morphology of the samples was analyzed using HR-TEM (JEOL-JEM-2100) at 200 kV. For the electrochemical measurements, the experiments were performed using Volta-lab40 (Tacussel Radiometer PGZ-401) potentiostat. The three-electrode system was applied under the effect of aggressive corrosion solution (1 M HCl) where the coated carbon steel set as a working electrode was vertically aligned with platinum, and saturated calomel electrode (SCE) electrode were utilized as auxiliary and a reference electrode, respectively. The polarization curves were obtained with a scan rate of 1 mV s^{-1} by sweeping the potential from −1000 to −200 mV. To achieve reproducibility, we done four parallel experiments for each prepared sample. EIS experiments were conducted in a frequency range with low limit 5×10^{-2} and high limit 10^5 Hz. The different frequency with a capacity of 10 MV peak-to-peaks was investigated using AC signals at open circuit potential.

3. RESULTS AND DISCUSSION

3.1. FTIR characterization

The typical FTIR curves of Ox-MWNTs and PASP/Ox-MWNTs are shown in Fig. 1. Ox-MWNTs (curve a) appeared several peaks at 1630 cm^{-1} of C=C conjugation system stretching, while peaks at 1726 cm^{-1} and 1748 cm^{-1} related to C=O stretching and the small broadband stretching of O–H at 3420 cm^{-1} are attributed to presence carboxylic group on carbon skeleton due to the oxidation effect [26]. The curve b confirmed formation of the PASP/Ox-MWNTs by revealing the presence of characteristics peaks of PASP at 1023, 1408, 1470 and 1588 cm^{-1} refer to C-O stretching vibration, $=CH_2$ bending vibration, -NH bending vibration of primary amine and C=O stretching in amide (-CONH-) structure, respectively [25]. The other observed peaks at 2978 and 2839 cm^{-1} are corresponding to the C-H stretching vibration of $-CH_2$ [33]. The previous reported works had confirmed that the PASP structure observed strong broadband peak at 3446.58 cm-1 due to presence of -NH -OH groups inside polymer chain structure [25, 33]. However, this peak is totally disappeared at PASP/Ox-MWNTs composite spectrum may be due to NH groups had been completely interacted with carboxylic or groups of Ox-MWNTs which in turn lead to the formation of amide bonds, proved from the newly observed peak at 1588 cm^{-1}.

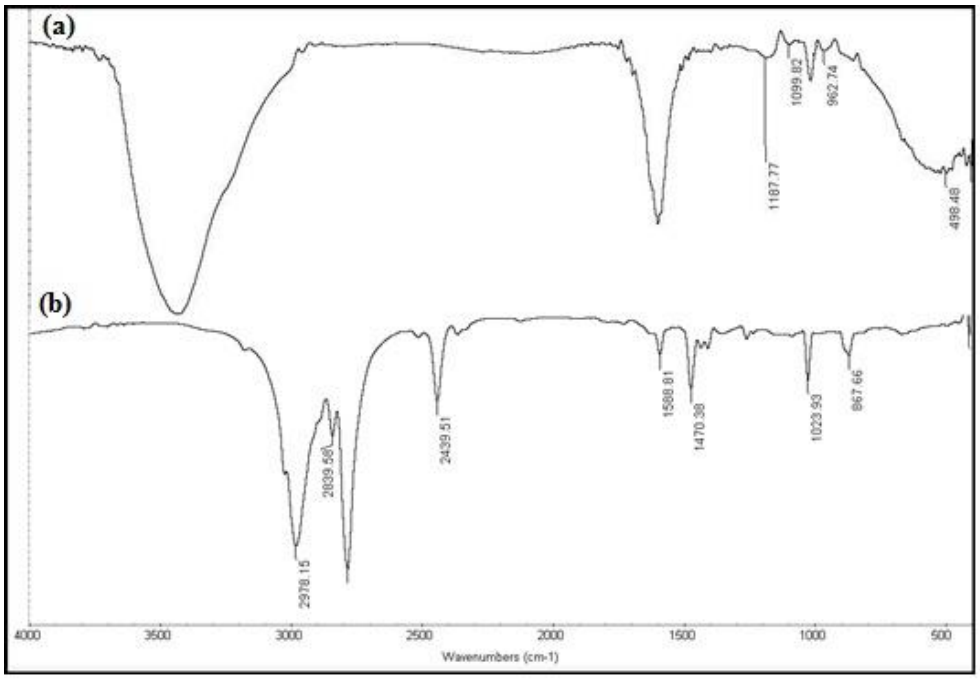

Figure 1. *FTIR* Curves of (a) Ox-MWNT and (b) PASP/Ox-MWNTs

3.2. TEM morphological characterization

The dispersion of the bulky PASP on the outer surface of Ox-MWNTs is due to the covalent interactions which maintain a good connection with the deformed Ox-MWNTs skeleton. Fig. 2(b) shows the PASP coiling out around the Ox-MWNTs edifying the highest possible linkage. This encapsulation allows a uniform distribution of polyaspartic acid due to the surrounding hydrophilic groups (C=O, NH, OH). In this situation, the competition driven by the applied voltage on the uniform distributed units towards coating in the electrolytic system would be equivalent. As clear from mentioned figure Ox-MWNTs bonded firstly with PSAS due to the formation of an amide bond, confirmed by FTIR analysis. In a second step, because PSAS possess many amine groups, several of Ox-MWNTs linkages to one chain of polyaminoacids. Third, the as known surface of Ox-MWNTs carries many carboxylic groups that work to link polyaminoacid series together forming a network-like configuration.

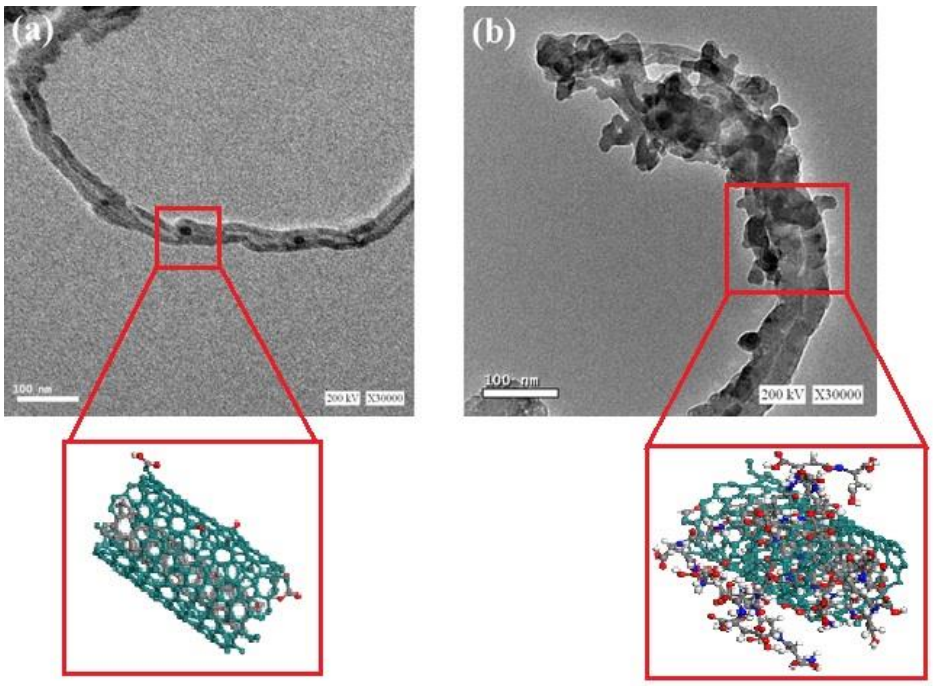

Figure 2. (a) TEM image of Ox-MWNTs and (b) TEM image of PASP/Ox-MWNTs

3.3. TGA Analysis

Figure 3 shows the thermal gravimetric analysis (TGA) of the parent and PASP/Ox-MWNTs. The typical thermal degradation of Ox-MWNTs shows excellent thermal stability extended up to around 600 ^{0}C followed by 30% weight loss due to the skeleton breakage from 600 - 800 ^{0}C. On the other hand, the mass reduction of the well-dried PASP/Ox-MWNTs sample starts at 100 ^{0}C due to the thermally evaporated water droplets making 4.6% weight loss. The second strong weight loss stage appears at temperature range 200 - 300 ^{0}C. It can be argued that this reduction temperature corresponds to the decomposition of PASP [34]. The remaining weight percent at the end of this stage corresponds to the percent of MWVTs whose breakdown starts latterly at about 620^{0}C [26]. This thermal pattern reveals that the PASP/Ox-MWNTs loading percentage of 4:1.

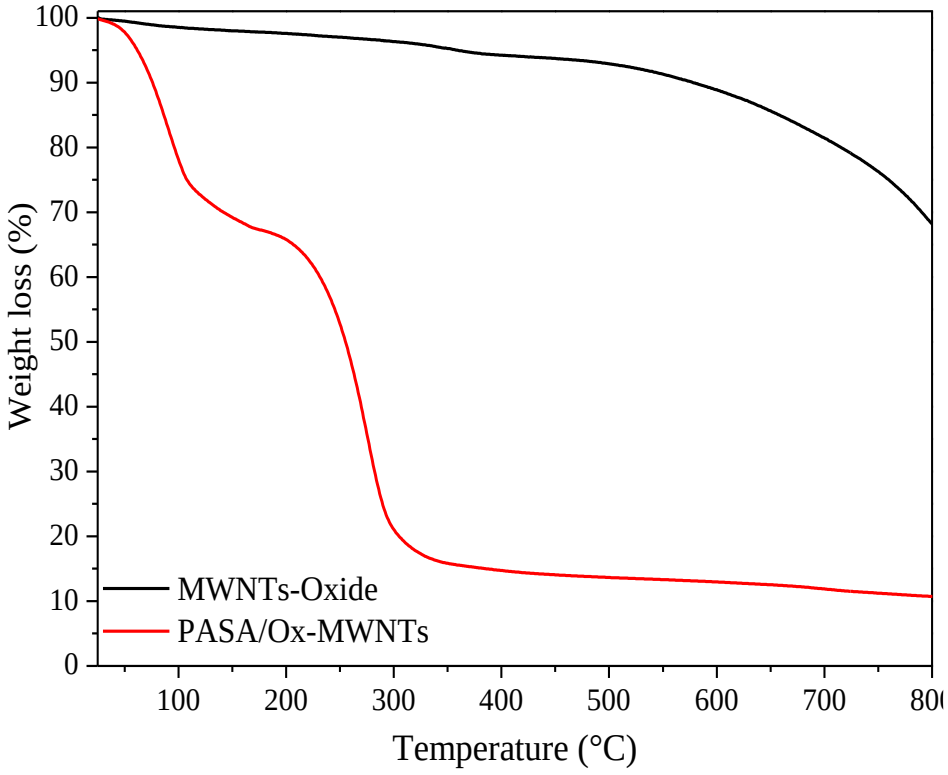

Figure 3. TGA Curves of Ox-MWNTs and PASP/Ox-MWNTs

3.4. Thickness calculation of electrodeposited layer

Electrodeposition process occurred on the carbon steel surface due to the prepared composite has unreacted terminal negatively charged groups (COO-) as mentioned at the experimental section. The thickness of the uniform electro-precipitated layers was calculated according to the following equations:

$$N_e = I \times t \times C \quad \ldots\ldots (1)$$

Where: N_e Number of electrons of aspartic molecule loss at distinct volt, I is a current in ampere measured for every applied volt, t is a time in second (it was 5 min), and C is 1 coulomb equal to 6.24 x 10^{18} electrons.

$$N_m = \frac{N_e}{S} \quad \ldots\ldots (2)$$

Where N_m is Number of the electrodeposited aspartic molecule and S number of electro-charged groups in one aspartic molecule (it equal to 2)

$$N_{el} = \frac{A}{r\,h} = \frac{1}{7.5 \times 10^{-6} \times 50 \times 10^{-4}} \quad \ldots\ldots (3)$$

Where N_{el} is a number of electrodeposited PASP/Ox-MWNTs units in one layer at the examined surface area (A), *r* is the diameter of electrodeposited composite and *h* is CNTs length according to TEM characterization which was equal to 7.5 $\times 10^{-6}$ and 50 $\times 10^{-4}$ cm, respectively.

$$n = \frac{wt}{M_{wt}} = \frac{1}{1.33} \quad \ldots\ldots (4)$$

Where *n*, wt, and $M_{wt,}$ are a number of moles, weight and molecular weight of aspartic acid, respectively.

$$m = n \times N_A \quad \ldots\ldots\ldots (5)$$

Where m is a number of aspartic acid molecules, and N_A is Avogadro number.

$$v = \frac{CNTs_{wt}}{CNTs_d} = \frac{1}{2.1} \quad \ldots\ldots (6)$$

Where *v* is the volume of 1 g Ox-MWNTs, and $CNTs_d$ is the density of it.

$$N_{CNTs} = \frac{V}{V_u} = \frac{V}{\pi\, h\, r_o^2} = \frac{0.47}{\pi \times 50 \times 10^{-4} \times (4\times10^{-6})^2} \quad \ldots\ldots (7)$$

Where N_{CNTS} is a number of Ox-MWNTs units, V_u is *the* volume of one Ox-MWNTs unit where r_o is the diameter of Ox-MWNTs and h is CNTs unit length according to TEM characterization which was equal to 4×10^{-6} and 50×10^{-4} cm, respectively.

$$N_c = \frac{m}{N_{CNTs}} \quad \ldots\ldots (8)$$

Where N_c is a number of aspartic acid molecules linked with per unit of Ox-MWNTs, it equal to 2.27×10^9.

$$N_{ec} = \frac{N_m}{N_C} \quad \ldots\ldots (9)$$

Where N_{eC}, is a number of electrodeposited PASP/Ox-MWNTs units on the surface of carbon steel.

$$N_l = \frac{N_{ec}}{N_{el}} \quad \ldots\ldots (10)$$

Where $N_{l,}$ is a number of precipitated layers of the prepared composite.

$$d = N_l \times r/_2 \quad \ldots\ldots (11)$$

We divided on 2 to calculate the thickness of one side of the electrodeposited layer and the obtained data is listed in Table 2.

Table 2. The calculated thickness of electrodeposited PASP/Ox-MWNTs composite layer at different applied voltages (Sample-3V, Sample-6V, Sample-9V and Sample-12V) in 1 M HCl solution.

Sample No.	Potential (V)	Current × 10^{-2} (A)	N_{ec} × 10^{10}	N_l	d (μ)
1	3V	3.5	1.44	5.5×10^{2}	20.5
2	6V	7.0	2.88	1.11×10^{3}	41.1
3	9V	10.5	4.33	1.66×10^{3}	61.3
4	12V	14.0	5.76	2.21×10^{3}	81.9

3.5. OCP measurements

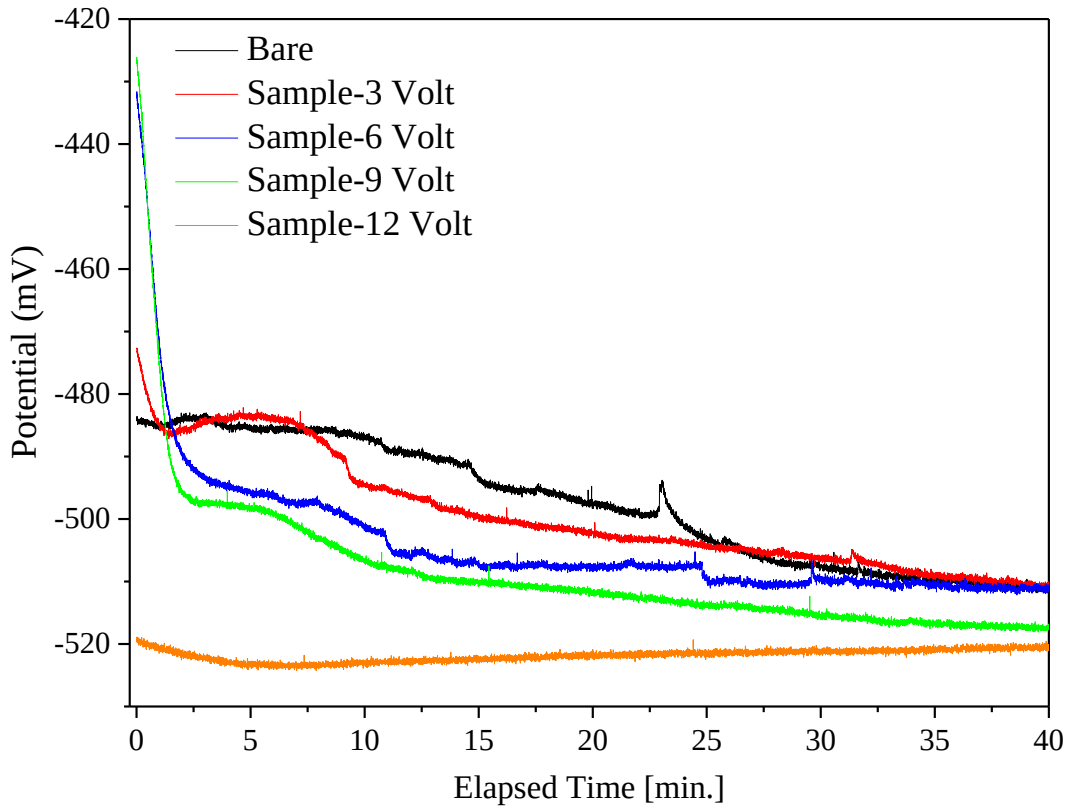

Figure 4. The obtained OCP values for the uncoated bare and coated carbon steel with PASP/Ox-MWNTs at different applied voltages (Sample-3V, Sample-6V, Sample-9V and Sample-12V) in 1 M HCl solution.

Fig. 4 indicates potential alternations against time for uncoated carbon steel electrode as well as coated samples with PASP/Ox-MWNTs. The OCP values for coated samples with PASP/Ox-MWNTs in different voltages were negatively shifted compared to the bare electrode, due to the PASP/Ox-MWNTs layer which is highly resistant to cathodic corrosion reaction. On the one hand, OCP value for the uncoated bar was obtained at -460 mV after it was exposed to 1 M HCl solution for the 2400 s. On the other hand, the OCP values of samples electroplated with PASP/Ox-MWNTs composite were

steadily increased to more negative potentials with progress in applied deposition voltage. As results observed, during the first 5 min of applying 12 V deposition potential, the OCP value achieved-520 mV, and it became regular after 24 min. By careful inspection of 3V and 6 V plots it could be shown that first the OCP values shifted undervalue of the carbon steel bar, however, after 34 min the OCP behavior became like as uncoated bar. This behavior is related to the high offensive rate of corrosive species over the metal surface due to the collapse of the protective layers. This result proves that below the critical electrical deposition field, the obtained protective layers were thinner than expected, which leads to easy penetration of aggressive molecules through its defects [35, 36].

3.6. Electrochemical impedance spectroscopy measurements

Electrochemical impedance spectroscopy (EIS) technique provides information about surface resistivity as well as the performance of the coating layer against the corrosive medium. EIS as Nyquist and bode curves for carbon steel bar and electrodeposited films of PASP/Ox-MWNTs with different voltages in HCl (1M) have been plotted in Fig. 5 and 6, respectively.

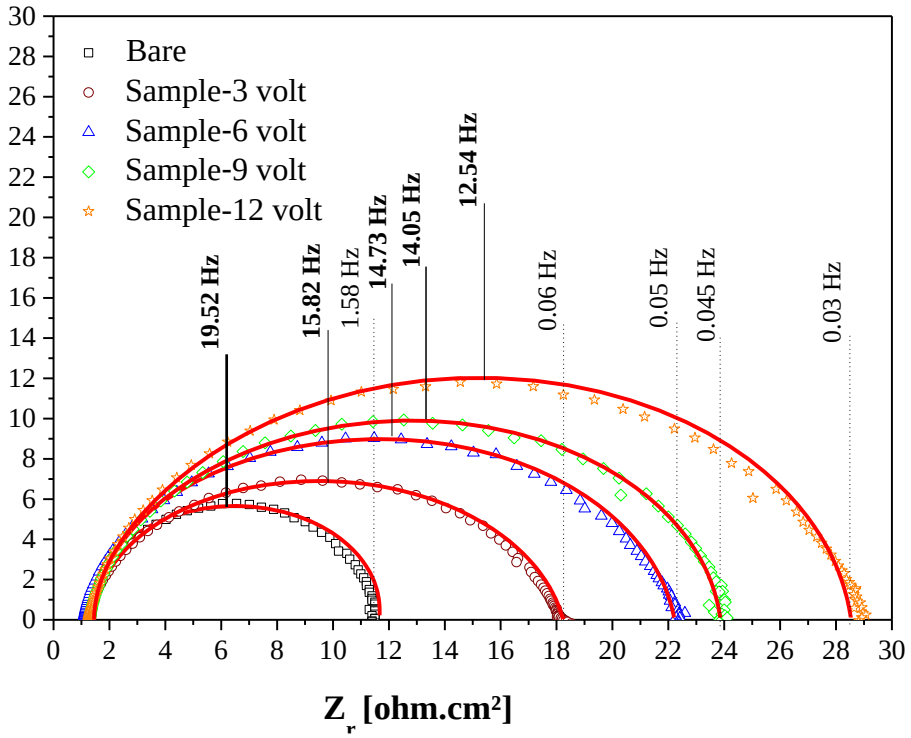

Figure 5. Nyquist plots of the uncoated bare and coated carbon steel with PASP/Ox-MWNTs at EIS method used to investigate the electrochemical degeneracy of metal and coating layer via potential and current with different applied electrochemical deposition voltage (Sample-3V, Sample-6V, Sample-9V and Sample-12V) in 1 M HCl solution.

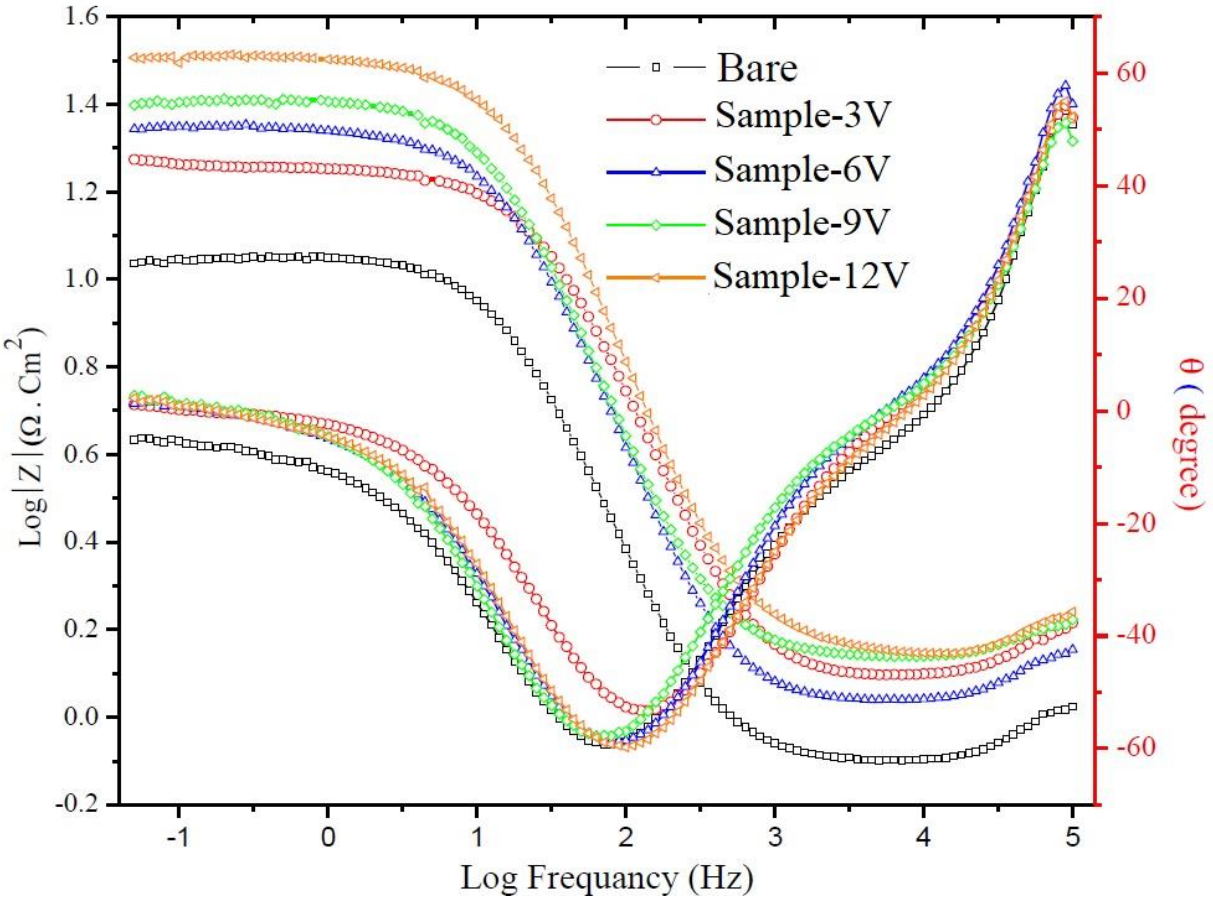

Figure 6. Bode plots of the uncoated bare and coated carbon steel with PASP/Ox-MWNTs at different applied voltages (Sample-3V, Sample-6V, Sample-9V and Sample-12V) in 1 M HCl solution.

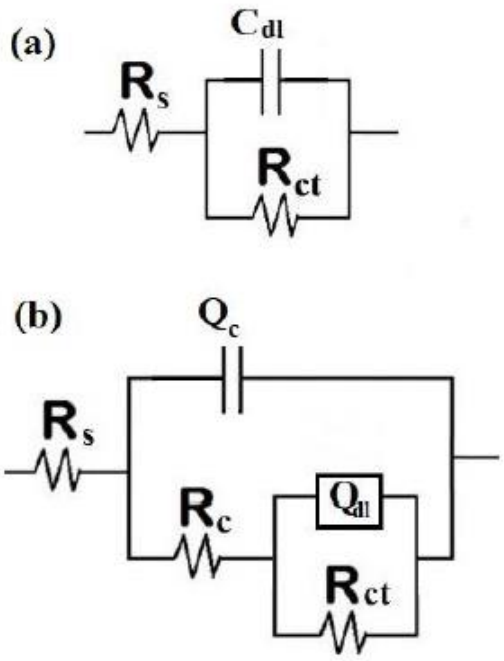

Figure 7. EEC of (a) uncoated bare and (b) electrodeposited coating of PASP/Ox-MWNTs on carbon steel at different applied voltages (Sample-3V, Sample-6V, Sample-9V and Sample-12V) in 1 M HCl solution.

The Nyquist curve is simplified in the relation between $Z_{imaginary}$ and Z_{real}, while bode plot is represented by double Y-axis (log Z_{real} and Θ degree) vs. log frequency. Significant parameters of EIS were assessed by fitting the obtained Nyquist curves to the electrical equivalent circuit (EEC) as shown in Fig. 7, the unpainted bare was fitted to the Randles model while the painted samples were fitted to R(C(R(QR) circuit [37]. The estimated factors are; solution resistance (R_s), coat capacitance (Q_c), double layer capacitance (Q_{dl}), charge transfer resistance (R_{ct}), coating resistance (R_c) and polarization resistance (R_p) are listed in Table 3. R_p is equal to the sum of all resistances of the circuit except R_s [38].

Table 3. EIS parameters of uncoated bar and electrodeposited PASP/Ox-MWNTs coatings on carbon steel surface in HCl (1M) at different applied voltages (Sample-3V, Sample-6V, Sample-9V and Sample-12V) in 1 M HCl.

Bare	R_s ($\Omega.cm^2$)		R_{ct} ($\Omega.cm^2$)		$C_{dl} \times 10^{-5}$ ($F.cm^{-2}$)		
	1.036		10.46		7.48		
Voltage	R_s ($\Omega.cm^2$)	$Q_c \times 10^{-8}$ ($F.cm^{-2}$)	R_{ct} ($\Omega.cm^2$)	N	$Q_{dl} \times 10^{-5}$ ($\Omega^{-1}. S^n$)	R_c ($\Omega.cm^2$)	η %
3 Volt	1.455	8.63	16.62	0.8581	5.01	1.532	37.06
6 Volt	1.382	4.31	19.29	0.7898	4.32	2.801	45.78
9 Volt	1.461	2.89	20.11	0.7447	3.94	3.906	47.99
12 volt	1. 457	2.16	23.83	0.7422	3.25	4.398	56.11

Q_{dl} is expressed by constant phase elements (CPE) due to the presence of quantifies different physical phenomena like surface in heterogeneity and its values ranging from −1 to 1, depending on n value, it be resistance when (n = 0), capacitance (n = 1), inductance (n =−1) or Warburg behavior (n = 0.5) [39, 40]. The Q_c values are calculated from the following law:

$$Q_c = \frac{\varepsilon_o \times \varepsilon}{d} \times A \qquad \ldots\ldots (12)$$

Where, the permittivity of space (ε_o) equal to 8.85×10^{-14} F/cm and dielectric constant (ε) is related to MWCNTs-Oxide because it mainly utilized to enhance electrical properties of other materials such as metal oxide, conducting polymer and as in our case amino acid. Average of MWCNTs-Oxide relative permittivity equal to 2000 [41]. Q_{dl} values are determined from EIS data fitness according to the following equation [42]:

$$Q_{dl} = 1/ Z_{CEP} = Q^o \times (j\,\omega)^n \qquad \ldots\ldots (13)$$

Where Q^o is coefficient of combination properties related to the surface and an electro-active species, j is an imaginary number ($j^2 = -1$), ω is the angular frequency ($\omega = 2\pi f$, f: frequency of Z_{CPE}).

$$\eta_{\%} = \left(1 - \frac{R_{ct\ bare}}{R_{ct\ coated\ sample}}\right) \times 100 \qquad \ldots\ldots (14)$$

As clarified from Figure 5 and Table 3, by amplifying electroplating voltage of the PASP/Ox-MWNTs composite on the carbon steel surface, values of R_{ct} and R_c increased, in contrary to the decreased Q_{dl} and Q_c values. It is important to note that the remarkable magnification of R_{ct} is attributed to PASP/Ox-MWNTs layer which enhanced the barrier effect by hindering the movements of aggressive ions before they pass to the metal substrate. The radius of curves at maximum frequencies determines the inhibition degree of electrochemical reactions which prevent the contact at the metal surface/corrosive molecules interface. The PASP/Ox-MWNTs electrodeposited sample at 12 V gives the maximum R_{ct} value where it promoted from 10.46 Ω for bare carbon steel to 23.83 Ω in the best. Bode plots Fig. 8 illustrated that $|Z_{real}|$ values of deposited PASP/Ox-MWNTs coatings at 12V was higher than their counterparts electroplated layers, this superior preform can be interpreted as follows; PASP/Ox-MWNTs nanoparticles are uniformly deposited in parallel to each other leading to protection of the metal surface as well as possible. The obtained EIS measurements are consistent with potentiodynamic polarization results. The coating layer efficiency (η %) against corrosion was measured from R_{ct} values according to the following equation [43, 44].

It was obvious that the η increases to 56.11 % when 12 V is applied for deposition of PASP/Ox-MWNTs layer on the carbon steel substrate surface.

3.7. Potentiodynamic polarizations

Potentiodynamic polarization plots of the untreated electrode compared with the electroplated carbon steel with PASP/Ox-MWNTs electrodes at different deposition voltages are shown in Fig. 8. The kinematic corrosion parameters values represented in corrosion potential (*Ecorr*), corrosion current (I_{corr}), and corrosion rate (C_R) which they are calculated and recorded in Table 4.

Table 4. Potentiodynamic parameters of uncoated bar and electrodeposited PASP/Ox-MWNTs coatings on carbon steel surface at different applied voltages (Sample-3V, Sample-6V, Sample-9V and Sample-12V) in 1 M HCl.

Voltage	**$-E_{corr}$ (mV)**	**R_p Ω.cm²**	**B_a (mV. dec⁻¹)**	**$-B_c$ (mV. dec⁻¹)**	**I_{corr} (mA/cm²)**	**C_R (mm/y)**	**η %**
Bare	460	10.46	94	152	2.4133	27.93	…..
3 Volt	454	18.15	91	151	1.3660	15.80	43.40
6 Volt	458	22.09	92	148	1.1226	12.99	53.48
9 Volt	484	24.02	91	139	0.9988	11.56	58.61
12 Volt	490	28.23	98	125	0.8487	9.82	64.83

The *Icorr* is calculated according to Stearn-Geary equation [45]:

$$I_{corr} = \frac{B}{R_p} = \frac{B_a.B_c}{2.303\,(B_a + B_c)\,R_p} \quad \ldots\ldots (15)$$

Where R_P obtained (from EIS measurements, b_a and b_c are the anodic and cathodic slopes ($\Delta E/\Delta \log I$), respectively. C_R was calculated as follows [46]:

$$C_R = \frac{I_{corr}\ (A.cm^{-2}).\ M\ (g)}{D\ (g.\ cm^{-2}).\ V} \times 3270 \qquad \ldots\ldots (16)$$

Where M is the molecular weight, V is the valence, D is the density of iron, and 3270 is a constant. As seen from Potentiodynamic curves, PASP/Ox-MWNTs electrodeposited carbon steel samples appear shifted negatively respecting to E_{corr} while I_{corr} values which significantly diminished in comparison with uncoated carbon steel. The PASP/Ox-MWNTs electroplated sample at 12 V gives the lowest corrosion potential value ≈ -490 mV while it was -460 mV for bare carbon steel. Values of E_{corr} indicate that the higher E_{corr} value toward the negative direction, the greater the inhibition of the cathodic reaction. PASP/Ox-MWNTs electroplated sample at 12V has shown remarkable diminish in the corrosion rate value when compared with unpainted carbon steel, where I_{corr} values were reduced from 2.4133 to 0.8487 mA/cm^{-2}. Therefore, it is possible to infer that, the presence of PASP/Ox-MWNTs layer enhanced the metal surface resistance against corrosion. The corrosion protection properties of PASP/Ox-MWNTs layer over carbon steel are attributed to its particular surface area, unique mechanical characteristics which restricted the permittivity of corrosive ions to the metal surface [47, 48]. The protective efficiencies (η %) of the electrodeposited layers were studied according to the next equation:

$$\eta_{\%} = \left(\frac{i_b - i_{b+c}}{i_b}\right) \times 100 \qquad \ldots\ldots (17)$$

Where i_b and i_{b+c} are the densities of corrosion current per unit area of untreated and treated samples, respectively. It is obvious that η value increased to 64.83 % when 12 V was applied for PASP/Ox-MWNTs deposition on the metal surface. The corrosion rate (C_R) is considered to be the most critical parameter which measured by potentiodynamic polarization technique [49]. By comparing C_R values for the coated samples, it is clear that the C_R diminished with amplifying the applied voltage where the obtained results were 15.80, 12.99, 11.56 and 9.82 mm/y for 3, 6, 9 and 12 deposition voltages respectively. The significant decrease in C_R could be interpreted by the presence of PASP/Ox-MWNTs as barrier layer "barrier effect" on the metallic surface which impeded the diffusion paths of corrosive molecules to the carbon steel surface [42]. The corrosion process of the carbon steel includes multi-stages; the main one depends on corrosive molecules (O_2 and H_2O)/metal surface contact. That means the protective layer becomes more efficient as anti-corrosive coating via its capability to prohibit O_2 and H_2O molecules from reaching to the metal surface [49, 43]. OCP measurements are compatible with Potentiodynamic results where optimize deposition potential (12 V) restricted propagation tracks of water and oxygen more than any applied voltages.

Depends on pervious reported work, PASP achieved η % equal to 45 % in seawater with total salinity 36841 ppm [50]. However, we utilized 1 M HCl as aggressive medium, the electrochemically deposited PASP/Ox-MWCNT composite gave 43.40 % enhanced to 64.83 % with increasing in applied electrodepositing voltage.

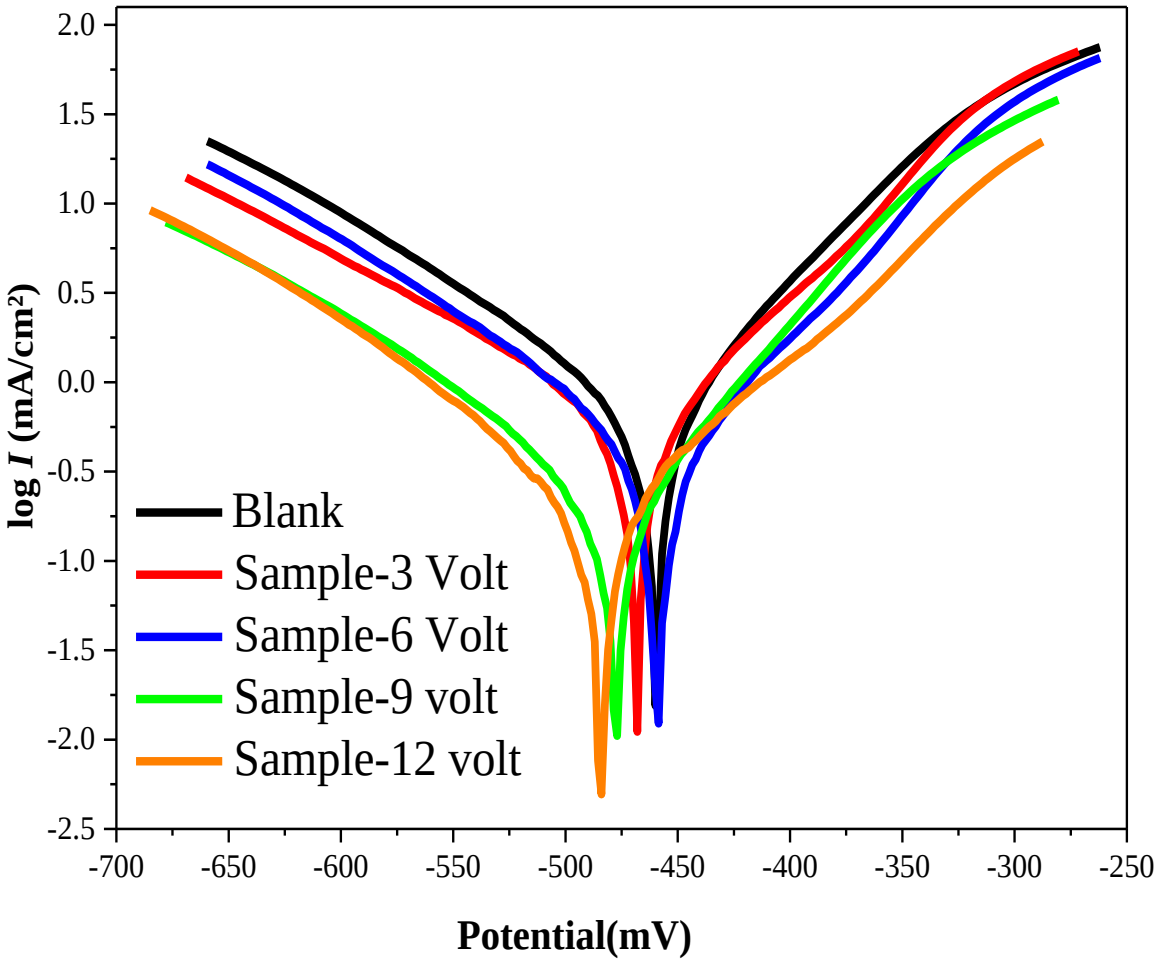

Figure 8. Potentiodynamic plots of the uncoated bare and coated carbon steel with PASP/Ox-MWNTs at different applied voltages (Sample-3V, Sample-6V, Sample-9V and Sample-12V) in 1 M HCl solution.

3.8. SEM surface analysis

Fig. 9 a,b and d show SEM of (a) carbon steel surface before exposure to corrosive medium (b) unprotected bar (c) protected bar at the optimum volt, after immersion 48 hr in a corrosive solution 1 M HCl. As clear from SEM pictures, Fig. 9b, the characterized surface of carbon steel has been destroyed after exposing to the aggressive solution. Dissolved oxygen, water molecules permeation, and attractive Cl^- offense the outer surface causing Fe oxidation for rust formation. The following equations indicate that ferrous chloride formed on the surface and consequently oxidized to ferric oxide (rust layer) [19].

$Fe^{2+} + 2Cl^- \rightarrow FeCl_2$ …….. (1)

$H_2O + O_2 + FeCl_2 \rightarrow 2H^+ + 2Cl + FeO_3$ …… (2)

Figure 9c shows the morphology of PASP/Ox-MWNTs coated carbon steel scratched at defects of PASP/Ox-MWNTs film, while the most steel surface left unscratched. SEM analysis proved that PASP/Ox-MWNTs layer does not entirely damage, these obtained data confirm the ability of

PASP/Ox-MWNTs film to hinder of the aggressive chloride and oxygen ions from penetrating the under the coating layer.

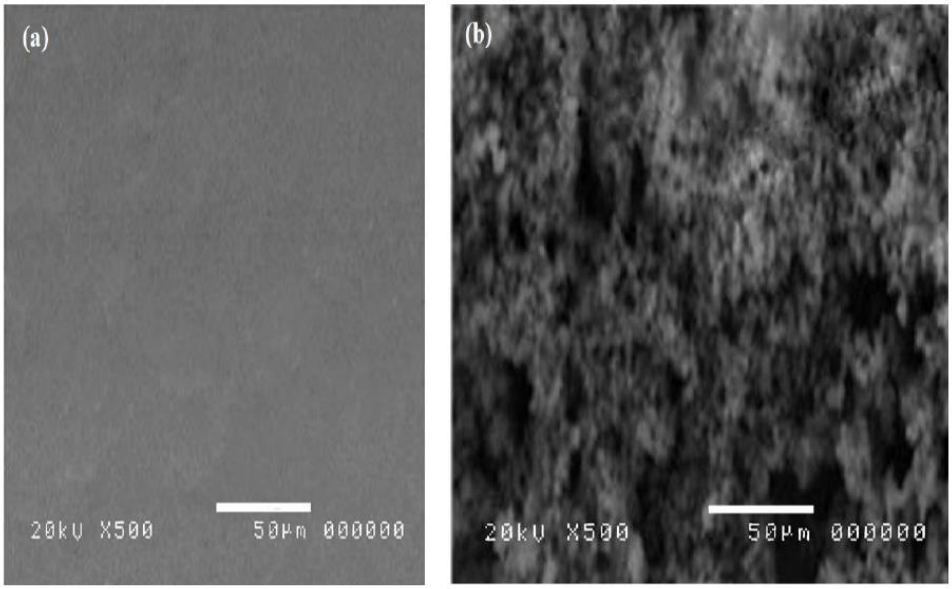

Figure 9. SEM of (a) uncoated bare before exposure to a corrosive solution and (b) uncoated bar after exposure to a corrosive solution 1 M HCl for 48hr.

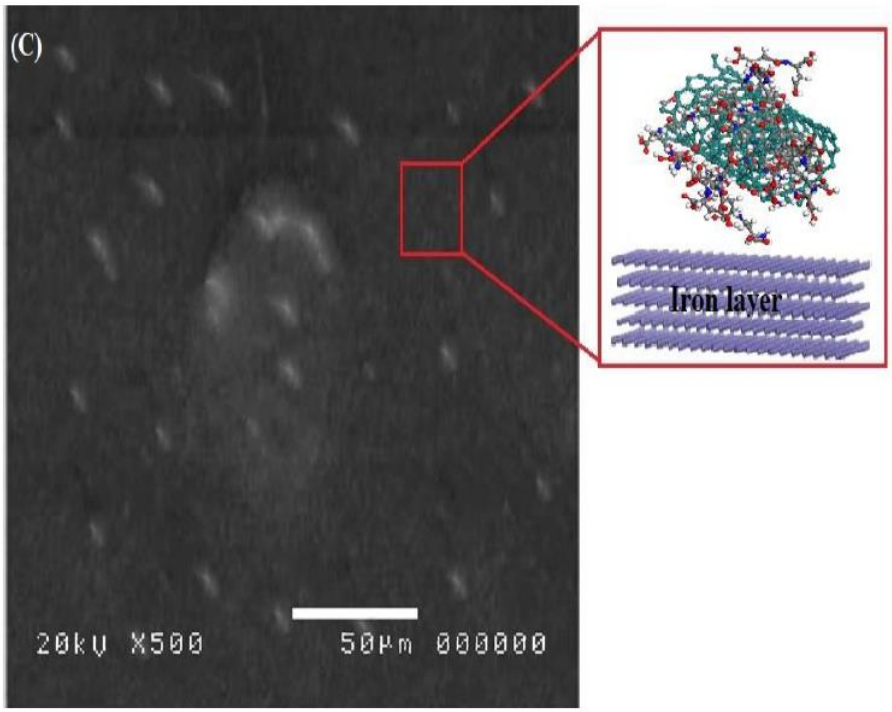

Figure 9c: SEM of PASP/Ox-MWNTs coated bar (electrodeposition volt =12) after exposure to a corrosive solution 1 M HCl for 48hr.

4. CONCLUSIONS

In this work, the capacity of PASP/Ox-MWNTs film as a protecting layer to avoid corrosion of carbon steel has been contemplated. All outcomes affirmed that PASP/Ox-MWNTs film protected the carbon steel because the deposited layer is very much framed on its surface and go about as a boundary defender. Notwithstanding the erosion insurance part of aspartic is recognized as on account of our current investigations, we might want to think about the imperfections on the Qx-MWNTs surface which might go about as the consumption start locales. So, in our future investigations, we concentrate on raising the estimation of consumption protection of carbon steel by changing the Ox-MWNTs surface by amino-acid anti-corrosive particles.

ACKNOWLEDGMENTS
The authors gratefully acknowledge EPRI for providing facilities for this work.

References

1. C. Carboni, P. Peyre, G. Béranger, C. Lemaitre, *J. Mater. Sci.*, 37 (2002) 3715-3723.
2. A.U. Malik, S. Ahmad, I. Andijani, S. Al-Fouzan, *Desalination*, 123 (1999) 205-213.
3. A.A. Abd-Elaal, N.M. Elbasiony, S.M. Shaban, E.G.Zaki, *J. Mol. Liq*., 249 (2018) 304-317.
4. M.A. Migahed, A.M. Al-Sabagh, E.A. Khamis, E.G.Zaki, *J. Mol. Liq*., 212 (2015) 360-371.
5. L. Lv, S. Yuan, Y. Zheng, B. Liang, S.O. Pehkonen, *Ind. Eng. Chem. Res.*, 53 (2014) 12363-12378.
6. K.S. Suganthi, K.S. Rajan, *Energy Convers. Manage*., 96 (2015) 115-123.
7. Y.B. Tao, C.H. Lin, Y.L. He, *Energy Convers. Manage*., 97 (2015) 103-110.
8. M. Prato, K. Kostarelos, A. Bianco, *Acc. Chem. Res*., 41 (2008) 60-68.
9. Y.-P. Sun, K. Fu, Y. Lin, W. Huang, *Acc. Chem. Res*., 35 (2002) 1096-1104.
10. D. Tasis, N. Tagmatarchis, A. Bianco, M. Prato, *Chem. Rev*., 106 (2006) 1105-1136.
11. J. Chen, *Science*, 282 (1998) 95-98.
12. M. Shanbedi, S.Z. Heris, A. Amiri, M. Baniadam, *J. Dispersion Sci. Technol*., 35 (2014) 1086-1096.
13. A. Amiri, M. Shanbedi, H. Amiri, S.Z. Heris, S.N. Kazi, B.T. Chew, H. Eshghi, *Appl. Therm. Eng*., 71 (2014) 450-459.
14. C. Backes, A. Hirsch, Chemistry of Nanocarbons, John Wiley & Sons, Ltd2010, pp. 1-48.
15. M. Á. Herranz, N. Martin, Noncovalent functionalization of carbon nanotubes, Wiley-VCH Verlag GmbH & Co. KGaA, (2010), Weinheim, Germany.
16. P. Chun Ke, Phys. Chem. *Chem. Phys*., 9 (2007) 439-447.
17. L. Vaisman, H.D. Wagner, G. Marom, *Adv. Colloid Interface Sci*., 128-130 (2006) 37-46.
18. S.S. Karajanagi, H. Yang, P. Asuri, E. Sellitto, J.S. Dordick, R.S. Kane, *Langmuir*, 22 (2006) 1392-1395.
19. H. Xie, A. Ortiz-Acevedo, V. Zorbas, R.H. Baughman, R.K. Draper, I.H. Musselman, A.B. Dalton, G.R. Dieckmann, *J. Mater. Chem*., 15 (2005) 1734.
20. A. Star, D.W. Steuerman, J.R. Heath, J.F. Stoddart, *Angew. Chem. Int.* Ed., 41 (2002) 2508-2512.
21. M. Zheng, A. Jagota, E.D. Semke, B.A. Diner, R.S. Mclean, S.R. Lustig, R.E. Richardson, N.G. Tassi, *Nature Materials*, 2 (2003) 338-342.
22. R.H. Baughman, *Science*, 297 (2002) 787-792.

23. M.J. O'Connell, P. Boul, L.M. Ericson, C. Huffman, Y. Wang, E. Haroz, C. Kuper, J. Tour, K.D. Ausman, R.E. Smalley, *Chem. Phys. Lett*., 342 (2001) 265-271.
24. A. Star, J.F. Stoddart, D. Steuerman, M. Diehl, A. Boukai, E.W. Wong, X. Yang, S.-W. Chung, H. Choi, J.R. Heath, *Angew. Chem. Int*. Ed., 40 (2001) 1721-1725.
25. M. Shanbedi, S. Z. Heris, A. Amiri, E. Hosseinipour, H. Eshghi, S.N. Kazi, *Energy Convers. Manage*, 105 (2015) 1366-1376.
26. K.I. Kabel, A.A. Farag, E.M. Elnaggar, A.G. Al-Gamal, *ARAB. J. SCI. ENG.* 41 (2016) 2211-2220.
27. G. D. Bennett, *Green Chem*., 82 (2005) 1380-1381.
28. Koskan, L. P.; Low, K. C. Polyaspartic Acid Scale Inhibitors. U.S. Patent 5,116,513, 1992.
29. M.L. Toebes, J.M.P. van Heeswijk, J.H. Bitter, A.J. van Dillen, K.P. de Jong, *Carbon,* 42 (2004) 307–315.
30. Y.-C. Chiang, W.-H. Lin, Y.-C. Chang, *Appl. Surf. Sci*., 257 (2011) 2401–2410.
31. C.L. Allen, A.R. Chhatwal, J.M.J. Williams, *Chem. Commun.,* 48 (2012) 666-668.
32. S. J. An, Y. Zhu, S. H. Lee, M. D. Stoller, T. Emilsson, S. Park, A. Velamakanni, J. An, and R. S. Ruoff, *J. Phys. Chem. Lett*., 1 (2010) 1259–1263.
33. P. Ji, M. Yang, W. Feng, *AIChE J.*, 57 (2011) 772-777.
34. S. Sharma, A. Dua, A. Malik, Eur. *Polym. J.* 59 (2014) 363-376.
35. M. Bagherzadeh, Z.S. Ghahfarokhi, E.G.Yazdi, *RSC Advances,* 6 (2016) 22007-22015.
36. C. Liu, F. Su, J. Liang, *Appl. Surf. Sci*., 351 (2015) 889-896.
37. Z. Zhang, N. Tiana, W. Zhang, X. Huang, L. Ruan, L. Wu, *Corros. Sci*., 111(2016) 675-689.
38. R.M. Bandeiraa, J.v. Drunenb, F. A. D-S. Ferreirac, U. P. Rodrigues-Filhoc, G. Tremiliosi-Filho, *Corros. Sci.*, 139 (2018) 35–46.
39. G. Gupta, N. Birbilis, A.B. Cook, A.S. Khanna, *Corros. Sci*., 67 (2013) 256-267.
40. S. Sathiyanarayanan, S. Syed Azim, G. Venkatachari, *Synth. Met*., 157 (2007) 205-213.
41. Q. Li, Q. Xue, L. Hao, X. Gao, Q. Zheng, *Compos. Sci. Technol*., 68 (2008) 2290–2296.
42. A. A. Farag, M.R. Noor El –Din, *Corros. Sci.*, 64 (2012) 174–183.
43. C.-H. Chang, T.-C.Huang, C.-W.Peng, T.-C.Yeh, H.-I.Lu, W.-I.Hung, C.-J.Weng, T.-I.Yang, J.-M.Yeh, *Carbon*, 50 (2012) 5044-5051.
44. A. Da Silva, J. Gomes, E. D'Elia, M. Rezende, A. Pinto, B. Silva, B. Silva, *Int. J. Electrochem. Sci.*, 8 (2013) 9317-9331.
45. M. Stern and A. L. Geary, *J. Electrochem. Soc*., 104 (1957) 56
46. T.-C. Huang, T.-C.Yeh, H.-Y.Huang, W.-F.Ji, T.-C.Lin, C.-A.Chen, T.-I Yang, J.-M.Yeh, *Electrochim. Acta*, 63 (2012) 185– 191.
47. N.F. Atta, K.M. Amin, H.A. Abd El-Rehim, A. Galal, *RSC Adv*., 5 (2015) 71627-71636.
48. Y. Liu, J. Zhang, S. Li, Y. Wang, Z. Han, L. Ren, *RSC Adv*., 4 (2014) 45389-45396.
49. A.A. Farag, K.I. Kabel, E.M. Elnaggar, A.G. Al-Gamal, *Corros. Rev.*, 35 (2017) 85-94.
50. Y. Gao, L. Fan L. Ward, Z, Liu, *Desalination*, 365 (2015) 220–226.

© 2020 The Authors. Published by ESG (www.electrochemsci.org). This article is an open access article distributed under the terms and conditions of the Creative Commons Attribution license (http://creativecommons.org/licenses/by/4.0/).